

Approximate Bayesian Computation with Path Signatures

JOEL DYER
UNIVERSITY OF OXFORD

PATRICK CANNON
IMPROBABLE

SEBASTIAN M SCHMON
IMPROBABLE

June 24, 2021

Abstract

Simulation models of scientific interest often lack a tractable likelihood function, precluding standard likelihood-based statistical inference. A popular likelihood-free method for inferring simulator parameters is approximate Bayesian computation, where an approximate posterior is sampled by comparing simulator output and observed data. However, effective measures of closeness between simulated and observed data are generally difficult to construct, particularly for time series data which are often high-dimensional and structurally complex. Existing approaches typically involve manually constructing summary statistics, requiring substantial domain expertise and experimentation, or rely on unrealistic assumptions such as *iid* data. Others are inappropriate in more complex settings like multivariate or irregularly sampled time series data. In this paper, we introduce the use of path signatures as a natural candidate feature set for constructing distances between time series data for use in approximate Bayesian computation algorithms. Our experiments show that such an approach can generate more accurate approximate Bayesian posteriors than existing techniques for time series models.

1. Introduction

Simulation models are an increasingly popular tool in a broad range of scientific disciplines including cosmology (Alsing et al., 2018), economics (Geanakoplos et al., 2012), and the biological sciences (Christensen et al., 2015). A drawback of such models is that, while they are straightforward to sample from, their complexity typically does not allow for explicit evaluation of the associated likelihood function. For example, in agent-based economic models, the observable data is often an aggregate quantity of the system, with the states of the individual agents constituting a vast set of latent variables which must be marginalised over. Consequently, traditional approaches to statistical inference are infeasible and alternative likelihood-free inference (LFI) methods are usually adopted.

Many such approaches have been proposed. One of the most widely used LFI methods is approximate Bayesian computation (ABC) (Tavaré et al., 1997; Pritchard et al., 1999; Beaumont et al., 2002), in which the Bayesian posterior distribution is approximated by sampling parameters θ from a prior distribution and synthetic datasets \mathbf{x} from a stochastic simulator, with likelihood denoted $p(\mathbf{x} | \theta)$, and comparing the output \mathbf{x} with real data \mathbf{y} . If the simulator output is sufficiently ‘close’ to the observation, then θ is retained as a sample from the approximate posterior distribution, otherwise it is discarded.

However, measuring closeness between model outputs is known to be challenging, particularly for time series data, which can exhibit complex dependency structures and may be multivariate and sampled at irregular time intervals. A common approach is to attempt to distil important features of the data using summary statistics and compare these instead (see e.g. Prangle, 2018). In practice, informative summary statistics are difficult to craft, which presents a trade off—a poor choice can materially bias the algorithm away from the true posterior distribution, yet constructing a sufficiently powerful choice can require substantial domain expertise, problem insight, and costly experimentation (see e.g. Drovandi and Frazier, 2021, for a recent comparison of methods with and without summaries). In other approaches the engineering of summary statistics is bypassed altogether (Bernton et al., 2019; Park et al., 2016), though existing methods of this type are generally not suitable for time series models without further adjustment.

We present here two novel methods for performing ABC for time series models that bypass the difficult problem of manually constructing summary statistics. Our approach leverages so-called *path signatures*, a key object in the mathematics of rough path theory (see e.g. Lyons, 2014b). Signatures have been employed successfully in a variety of tasks, from hand-gesture recognition (Li et al., 2017) to the early identification of Alzheimer’s disease (Moore et al., 2019), and constitute a natural feature set for multivariate and even irregularly sampled sequential data (Salvi et al., 2020). We demonstrate that the path signature can be employed directly as a summary statistic, or in the context of a semi-automatic projection approach, to construct a powerful distance measure for time series data in ABC, and further that such an approach can recover more accurate posterior estimates than existing techniques.

1.1. Likelihood-free inference background

In this section, we will recapitulate some standard approaches to approximate Bayesian computation (ABC) with an emphasis on time series data. Let $\mathcal{S}_n(\mathbb{R}^d)$ be the space of all length n sequences taking values in \mathbb{R}^d and suppose we have time series data $\mathbf{y} = (y_{t_1}, y_{t_2}, \dots, y_{t_n}) \in \mathcal{S}_n(\mathbb{R}^d)$, observed at real times $0 < t_1 < t_2 < \dots < t_n$, and assumed to have been drawn from the generative model with density $p(\mathbf{y} \mid \boldsymbol{\theta})$ parameterised by $\boldsymbol{\theta} = (\theta^{(1)}, \dots, \theta^{(p)}) \in \Theta \subseteq \mathbb{R}^p$. Given a prior distribution $\pi(\boldsymbol{\theta})$ on Θ , the central object in Bayesian inference is the posterior distribution

$$\pi(\boldsymbol{\theta} \mid \mathbf{y}) \propto p(\mathbf{y} \mid \boldsymbol{\theta})\pi(\boldsymbol{\theta}). \quad (1)$$

For simulation models, the likelihood function $p(\mathbf{y} \mid \boldsymbol{\theta})$ is commonly intractable, in the sense that it cannot be evaluated point-wise, making infeasible standard Bayesian approaches to posterior inference such as Markov chain Monte Carlo (MCMC).

In such scenarios an established alternative is offered by ABC (Tavaré et al., 1997; Pritchard et al., 1999; Beaumont et al., 2002) which allows the user to approximate the true posterior (1) using only forward samples from the simulator. Broadly, the user is required to specify summary statistics $\mathbf{s} : \mathcal{S}_n(\mathbb{R}^d) \rightarrow \mathbb{R}^k$ and a distance metric ρ , and the true likelihood function is approximated as

$$\tilde{p}(\mathbf{s}(\mathbf{y}) \mid \boldsymbol{\theta}) = \int K_h[\rho(\mathbf{s}(\mathbf{y}), \mathbf{s}(\mathbf{x}))] \cdot p(\mathbf{x} \mid \boldsymbol{\theta}) \, d\mathbf{x}, \quad (2)$$

where $K_h(x) = K(x/h)/h$ is a kernel function with bandwidth parameter h . The resulting ABC posterior is then given by

$$\pi_{\text{ABC}}(\boldsymbol{\theta} \mid \mathbf{s}(\mathbf{y})) \propto \tilde{p}(\mathbf{s}(\mathbf{y}) \mid \boldsymbol{\theta}) \pi(\boldsymbol{\theta}), \quad (3)$$

which is consistent as $h \rightarrow 0$ if the employed summary statistic is sufficient, since as $h \rightarrow 0$, $K_h[\rho(\mathbf{s}(\mathbf{y}), \mathbf{s}(\mathbf{x}))] \rightarrow \delta_{\mathbf{y}}(\mathbf{x})$, and so the right hand side of Equation (2) approaches $p(\mathbf{y} | \boldsymbol{\theta})$. Additionally, extending upon the concept of generalized Bayesian inference (Bissiri et al., 2016; Knoblauch et al., 2019), Schmon et al. (2020) note that ABC can be seen as a generalized Bayesian method targeting the posterior

$$\pi_{\text{GBI}}(\boldsymbol{\theta} | \mathbf{y}) \propto \int e^{-w \cdot \ell(\mathbf{y}; \mathbf{x})} p(\mathbf{x} | \boldsymbol{\theta}) \pi(\boldsymbol{\theta}) d\mathbf{x} \quad (4)$$

for an arbitrary loss function $\ell(\mathbf{y}; \mathbf{x})$ that captures the discrepancy between observation \mathbf{y} and simulation \mathbf{x} .

The approach as presented above leaves open a plethora of possible choices for \mathbf{s} , ρ and $K_h(x)$ —or, more generally, the loss function ℓ —which has sparked great interest in the choice of those values in different scenarios, the complete enumeration of which is beyond the scope of this overview. However, we summarise here some of the most common approaches.

Rejection ABC The standard rejection ABC (REJ-ABC) algorithm corresponds to choosing a uniform kernel $K_\epsilon(d) \propto \mathbb{1}[d < \epsilon]$. That is, parameter values $\boldsymbol{\theta}$ are independently drawn from the prior and are retained as samples from an approximate posterior according to whether the distance d between $\mathbf{s}(\mathbf{y})$ and $\mathbf{s}(\mathbf{x})$ falls below a threshold ϵ . The choice of threshold ϵ is left to the experimenter, and for example may be determined in advance of the inference procedure, or chosen after simulation time such that a certain proportion of the total simulation budget is retained.

Semi-automatic ABC Fearnhead and Prangle (2012) propose a method for automatically generating low-dimensional summary statistics by reducing a larger candidate set of summaries, referred to as semi-automatic ABC (SA-ABC). Given a set of N training data points $(\mathbf{x}_i, \boldsymbol{\theta}_i) \sim p(\mathbf{x}, \boldsymbol{\theta})$, $i = 1, \dots, N$, and a candidate vector $\mathbf{g}(\cdot)$ of J summary statistics, the method proceeds by performing vector-valued linear regression from $\mathbf{g}(\mathbf{x}_i)$ to $\boldsymbol{\theta}_i$, producing a matrix A of coefficients. The summaries \mathbf{s} are then taken to be the output of this regression, i.e. $\mathbf{s}(\mathbf{x}_i) = A\mathbf{g}(\mathbf{x}_i)$. The motivation for this is that, under a quadratic loss, the optimal summary statistics can be shown to be the posterior mean $\mathbb{E}[\boldsymbol{\theta} | \mathbf{y}]$. A drawback of this method, however, is that it requires the construction of an initial set of candidate summaries, which would need to be informative. Other approaches in this vein include that of Nakagome et al. (2013), in which the authors propose the use of SA-ABC using kernel ridge regression, to exploit the nonlinearities induced by kernel methods in this regression task.

K2-ABC Park et al. (2016) propose double kernel ABC (K2-ABC), an ABC method that bypasses the problem of constructing summary statistics by using the maximum mean discrepancy (MMD) between kernel mean embeddings $\mu_{\mathbf{x}}$ and $\mu_{\mathbf{y}}$ of (a) the simulator density $p(\cdot | \boldsymbol{\theta})$ and (b) the true density giving rise to the observation \mathbf{y} , respectively. With a suitable kernel k , the discrepancy between the simulation output \mathbf{x} and observation \mathbf{y} is then taken to be the squared MMD

$$\text{MMD}^2 = \|\mu_{\mathbf{x}} - \mu_{\mathbf{y}}\|_{\mathcal{H}}^2, \quad (5)$$

where \mathcal{H} is the reproducing Kernel Hilbert space (RKHS) associated with k . In this way, the choice of summary statistics (e.g. as required in SA-ABC) can be seen as being replaced

by the choice of kernel k . For time series data, the authors suggest that the dependency structure can be ignored, and that the observation $\mathcal{Y} := \{y_i\}_{i=1}^n$ and simulation output $\mathcal{X} := \{x_i\}_{i=1}^m$ can be treated as iid data from the marginal densities \tilde{p}_θ and \tilde{q} , respectively. An unbiased estimate of the MMD, under this assumption, can thus be obtained as

$$\widehat{\text{MMD}}^2(\tilde{p}_\theta, \tilde{q}) = \frac{1}{m(m-1)} \sum_{\substack{x, x' \in \mathcal{X} \\ x' \neq x}} k(x, x') + \frac{1}{n(n-1)} \sum_{\substack{y, y' \in \mathcal{Y} \\ y' \neq y}} k(y, y') - \frac{2}{nm} \sum_{\substack{x \in \mathcal{X} \\ y \in \mathcal{Y}}} k(x, y). \quad (6)$$

Wasserstein ABC Bernton et al. (2019) propose a further method for measuring the discrepancy between observations and simulated data that circumvents the problem of manually constructing summary statistics. The approach uses as its measure of discrepancy the p -Wasserstein distance between the empirical distribution of observations $\mathbf{y} = (y_1, y_2, \dots, y_n) \in \mathbb{R}^n$ and simulated data $\mathbf{x} = (x_1, x_2, \dots, x_m) \in \mathbb{R}^m$, that is,

$$\mathcal{W}_p(\mathbf{y}, \mathbf{x})^p = \inf_{\gamma \in \Gamma_{n,m}} \sum_{i=1}^n \sum_{j=1}^m \rho_0(y_i, x_j)^p \gamma_{ij} \quad (7)$$

where ρ_0 is a distance on \mathbb{R} and $\Gamma_{n,m}$ is the set of $n \times m$ matrices with non-negative entries, columns summing to m^{-1} , and rows summing to n^{-1} . The authors propose to use $p = 1$, in order to make a minimal number of assumptions on the existence of moments of the data-generating process.

A number of solutions are proposed in Bernton et al. (2019) to account for the dependency structure inherent in time series data. The first strategy discussed is the use of *curve matching*, in which a time augmentation $y_{t_i} \mapsto (t_i, y_{t_i})$ is applied to the data, and the following ground distance between elements of the sequence used:

$$\rho_0((t_i, y_{t_i}), (t_j, x_{t_j}); \lambda) = \|y_{t_i} - x_{t_j}\| + \lambda |t_i - t_j| \quad (8)$$

where $\lambda > 0$ is a free parameter that interpolates the distance in (7) between the sum of Euclidean distances $\sum_i \|y_{t_i} - x_{t_i}\|$ and the Wasserstein distance between the empirical marginal distributions of \mathbf{y} and \mathbf{x} . A heuristic for tuning λ is offered only for the case of univariate \mathbf{y} and \mathbf{x} .

A second strategy employs *reconstructions*, where the data are transformed to generate empirical distributions that allow for easier identifiability of parameters. Two types of reconstructions are considered: delay reconstructions, which is a common technique for reconstructing phase spaces in dynamical systems theory that involves considering lagged sequences of observations from the data; and residual reconstructions, in which the data is transformed according to the structure of the generative model such that they become iid observations, for example by considering $\epsilon_t = (x_t - a x_{t-1}) / \sigma$ in the case of a centered AR(1) model with parameter $\theta = (a, \sigma)$. However, it is undesirable to rely on such methods. For the case of delay reconstructions, properly estimating the lag parameters is key to its success (Fraser and Swinney, 1986) and obtaining reliable estimates remains a significant challenge (Bradley and Kantz, 2015). This is likely to be exacerbated in likelihood-free inference (LFI) settings, in which time series are stochastic and are often short, due to computational expense. Delay reconstructions will then also further reduce this length of the data, which can be costly to the quality of the inference procedure. Furthermore, the often complicated or unknown internal mechanisms of complex simulation models typically do not allow for a simple transformation of the output into iid data, limiting the applicability of this approach in LFI settings.

2. Path signatures

There are currently few, if any, methods well-suited to performing approximate Bayesian inference for time series models. Existing approaches often make unrealistic assumptions such as iid data, or require the use of data transformations that are difficult to construct or that require substantially reducing the length of datasets, which may be prohibitively costly. Moreover, where solutions for time series are proposed, their discussion is often limited to univariate data, raising the question of whether methods exist that are robust to more general LFI settings, such as those involving multivariate and/or irregularly sampled data with missing values. To this end, we introduce the use of *path signatures* as a flexible and general framework for performing LFI for complex time series models, and provide an overview of their important properties in this section.

2.1. Path integrals and signatures

Following [Levin et al. \(2016\)](#), we first assume that $X: J \rightarrow E := \mathbb{R}^d$ is a d -dimensional path on a compact set J , e.g. $J = [0, T]$ for some $T > 0$. The path X is said to be of finite p -variation for $p \geq 1$ if

$$\|X\|_{p,J} := \left(\sup_{\mathcal{D}_J \subset J} \sum_l \|X_{t_l} - X_{t_{l-1}}\|^p \right)^{1/p} < \infty, \quad (9)$$

where $\sup_{\mathcal{D}_J \subset J}$ indicates that the supremum is taken over all finite partitions \mathcal{D}_J of J . We further denote by $\mathcal{V}^p(J, E)$ the set of continuous paths $X: J \rightarrow E$ of finite p -variation.

Definition 1 (Path Signature). *The signature of a path $X = (X^1, X^2, \dots, X^d): [0, T] \rightarrow \mathbb{R}^d$ of finite p -variation is an infinite collection of statistics that characterises the path up to a negligible equivalence class ([Bonnier et al., 2019](#)). It is defined by the infinite collection of statistics*

$$\text{Sig}(X) = (1, S(X)_{0,T}^1, S(X)_{0,T}^2, \dots, S(X)_{0,T}^d, S(X)_{0,T}^{1,1}, S(X)_{0,T}^{1,2}, \dots) \quad (10)$$

consisting of the m -fold iterated integral of X with multi-index i_1, \dots, i_m defined as

$$S(X)_{0,T}^{i_1, \dots, i_m} = \int_{0 \leq t_1 < \dots < t_m \leq T} \dots \int dX_{t_1}^{i_1} \dots dX_{t_m}^{i_m}. \quad (11)$$

Remark 1. *When the underlying path X is of bounded variation, i.e. $X \in \mathcal{V}^1([0, T], \mathbb{R}^d)$, the integral (11) can be understood as the Riemann-Stieltjes integral with respect to X . When the underlying path is not smooth, the integrals are taken to be stochastic or rough path integrals ([Chevyrev and Oberhauser, 2018](#)). For example, in the case of Brownian motion in \mathbb{R}^d , the integrals are stochastic and can be taken in the Stratonovich sense. For a larger class of stochastic processes, rough path theory ([Lyons, 2014a](#)) provides an integration theory that enables the computation of (11). As we will discuss later, this work considers throughout only linear interpolations between points in time series, so all paths considered here are of finite variation.*

Path signatures are thus infinite sequences of statistics for path-valued random variables, which capture information regarding the order of observations along the path and area

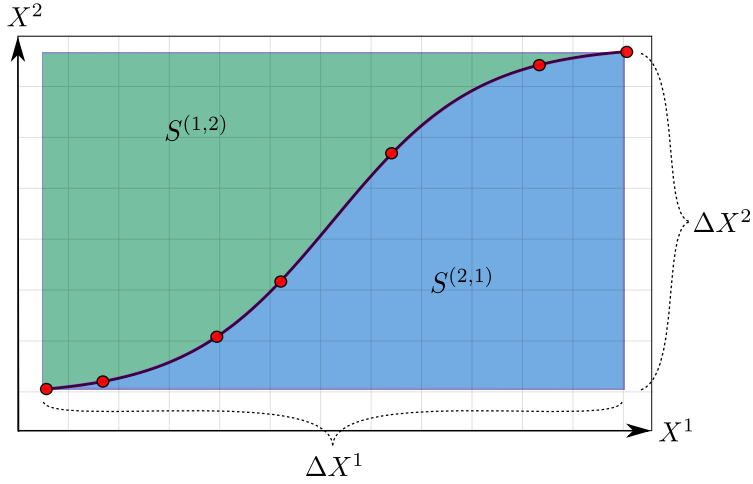


Figure 1.: A schematic demonstrating the geometric interpretation of signature terms for an example two-dimensional path. Red circles indicate the (possibly irregular) observations, and the black curve illustrates the underlying continuous path. Depth-1 terms correspond to the increments ΔX^1 and ΔX^2 , while the depth-2 terms $S^{(1,2)}$ and $S^{(2,1)}$ correspond to the green and blue areas, respectively.

enclosed by the path, and the interaction between different channels of the path. Figure 1 gives a geometric interpretation of the first two levels of the signature transform as the increments along each dimension and the areas bounded by the curve.

Remark 2. *The signature of a univariate path consists only of powers of the difference between the final and initial points in the stream (see e.g. Chevyrev and Kormilitzin, 2016, Example 5). Therefore in practice one always considers paths in at least two dimensions. This can always be achieved by including the observation time as a channel in the path.*

Signatures have a number of desirable properties. In particular, they enjoy *universal nonlinearity*: the signature terms capture all possible nonlinearities in multivariate time series data, in the sense that it is possible to approximate any nonlinear function of a path arbitrarily well with a linear functional of the signature (Király and Oberhauser, 2019, Theorem 1).

2.2. Signature Kernel

In light of their interesting properties, signatures represent a canonical feature transformation for sequential data. Explicit evaluation of the signature is however impossible, as it has infinitely many terms. As a result, it has been common in applications of the signature method to truncate the signature to some depth D , retaining all terms given by (11) for which $m \leq D$. This results in a loss of potentially important information in the stream, which may be partially overcome by combining the signature with neural networks, as described in Bonnier *et al.* (2019). In part to address this problem, recent years have seen the development of a characteristic signature kernel for sequential data and corresponding kernel trick. Before introducing the signature kernel, we first provide further details on the mathematical setup.

Definition 2 (Formal polynomials and power series). *Let V be a Banach space, and let*

$$V^{\otimes k} := \underbrace{V \otimes \cdots \otimes V}_k \quad (12)$$

denote the k -fold classical tensor product of V with itself. The space of formal polynomials and of formal power series over V are defined as

$$T(V) = \bigoplus_{k=0}^{\infty} V^{\otimes k} \quad \text{and} \quad T((V)) = \prod_{k=0}^{\infty} V^{\otimes k}, \quad (13)$$

respectively, where \oplus denotes the direct sum.

With these definitions in place, we now define an inner product on the space of formal polynomials, $T(V)$.

Definition 3 (Inner product on the space of formal polynomials). *Let V be a d -dimensional Banach space with canonical basis $\{e_1, \dots, e_d\}$. The elements*

$$\left\{ e_{i_1} \otimes e_{i_2} \otimes \cdots \otimes e_{i_k} : (i_1, \dots, i_k) \in \{1, \dots, d\}^k \right\} \quad (14)$$

form a basis of $V^{\otimes k}$. With an inner product on $V^{\otimes k}$ defined on basis elements given by

$$\langle e_{i_1} \otimes \cdots \otimes e_{i_k}, e_{j_1} \otimes \cdots \otimes e_{j_k} \rangle_{V^{\otimes k}} = \langle e_{i_1}, e_{j_1} \rangle_V \langle e_{i_2}, e_{j_2} \rangle_V \cdots \langle e_{i_k}, e_{j_k} \rangle_V, \quad (15)$$

an inner product between any pair of elements $A = (a_0, a_1, \dots)$, $B = (b_0, b_1, \dots)$ in $T(V)$ can be defined through the extension of the inner product $\langle \cdot, \cdot \rangle_{V^{\otimes k}}$ by linearity to

$$\langle A, B \rangle = \sum_{k=0}^{\infty} \langle a_k, b_k \rangle_{V^{\otimes k}}. \quad (16)$$

The path signature $\text{Sig}(X)$ of a path $X: [0, T] \rightarrow V$ is an element of the space of formal power series $T((V))$. Through Definition 3, we are now equipped with an inner product on this space and so can define the signature kernel.

Definition 4 (Signature kernel, [Király and Oberhauser \(2019\)](#); [Salvi et al. \(2020\)](#)). *Let $I = [u, u']$ and $J = [v, v']$ be two closed intervals, $C^1(I, V)$ be the space of continuously differentiable paths on the interval I with values in a d -dimensional Banach space V , and let $x \in C^1(I, V)$ and $y \in C^1(J, V)$. The signature kernel $k_{x,y} : I \times J \rightarrow \mathbb{R}$ is then defined as*

$$k_{x,y} : (s, t) \mapsto \langle \text{Sig}(x)_s, \text{Sig}(y)_t \rangle, \quad (17)$$

where

$$\text{Sig}(x)_s = (1, S(x)_{u,s}^1, S(x)_{u,s}^2, \dots, S(x)_{u,s}^d, S(x)_{u,s}^{1,1}, S(x)_{u,s}^{1,2}, \dots) \quad (18)$$

is the signature of the path x over the interval $[u, s]$ for $u \leq s \leq u'$. Throughout, we will write $k(x, y)$ as a shorthand for $k_{x,y}(u', v')$.

This signature kernel involves the *sequentialisation* of a static kernel $k^+ : V \times V \rightarrow \mathbb{R}$, in which the path x is first “lifted” into a path evolving in a feature space \mathcal{H} using k^+ , and the signature of this lifted path is used in the signature kernel. We refer the interested reader to [Király and Oberhauser \(2019\)](#) for further details.

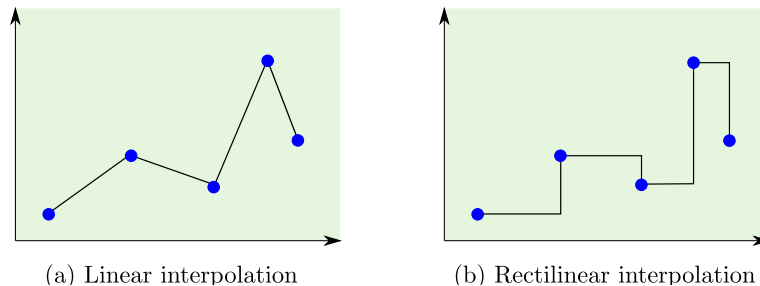


Figure 2.: Two interpolation schemes to convert a series of (blue) points into paths.

Using the signature kernel presents a difficulty as computing its value involves taking the inner product between two infinite-dimensional objects. For this reason the signature kernel has typically appeared as a truncated signature kernel, in which the inner product depends only on terms of the signature to some finite depth D (Király and Oberhauser, 2019; Toth and Oberhauser, 2019). In more recent work, Salvi et al. (2020) show that a kernel trick for the signature kernel—that is, evaluation of the inner product between the two full, untruncated signatures in Definition 4—corresponds to solving a Goursat partial differential equation, the solution to which may be obtained with standard finite element methods. In other words, while evaluation of the signature itself is impossible, the signature kernel is amenable to computation and this will form the basis of our novel ABC algorithms proposed in Section 3.

2.3. Path signatures in practice

In this section, we provide an overview of common steps involved in using path signatures in practical settings involving real-world data.

2.3.1. Pre-processing

As discussed above, the signature is defined on a continuous path. However, it is often desirable to use it in discrete settings, i.e. for time series consisting of samples from some underlying path (Xie et al., 2018; Bonnier et al., 2019; Morrill et al., 2020). In such cases, one usually constructs a path from a sequence \mathbf{y} of discrete observations using an interpolation scheme. Common interpolation schemes include piece-wise linear and rectilinear interpolations; see Figure 2 and Chevyrev and Kormilitzin (2016, Section 2).

Prior to implementing the chosen interpolation scheme, and depending on the nature of the data at hand, it is sometimes appropriate to apply a transformation to the data. The reason for doing so is that certain transformations may enable the signature to represent information in the stream more conveniently. A large set of such transformations have been proposed in the literature on inference using path signatures; see Morrill et al. (2020) for a recent summary and comparison of many of these. Here, we describe two of the most common pre-signature path transformations.

Cumulative sum Recall from Figure 1 that the depth 1 signature terms correspond to the increment along the path, and that a subset of the depth 2 terms correspond to the areas

above and below the curve. For certain data types, for example non-negative binary or spiking data, the data may not be well-characterised by these terms by default. In such cases it can be beneficial to consider instead the cumulative sum of the observations (Király and Oberhauser, 2019), which can intuitively be thought of as propagating information from earlier in the sequence to later in the stream, more readily exhibiting the structure of the stream. The effect of this can be to shift information into lower order terms in the signature, for example the increments (depth 1 terms).

Lead-lag transformation This transformation is a mapping $\phi : \mathcal{S}_n(\mathbb{R}^d) \rightarrow \mathcal{S}_{2n-1}(\mathbb{R}^{2d})$ transforming $\mathbf{x} = (x_1, x_2, \dots, x_n)$ into

$$\phi(\mathbf{x}) = ((x_1, x_1), (x_1, x_2), (x_2, x_2), \dots, (x_{n-1}, x_n), (x_n, x_n)). \quad (19)$$

Applying this transformation enables the signature to emphasise certain properties of the path such as the quadratic variation and the Lévy area when combined with the cumulative sum (Gyurk, 2014; Chevyrev and Kormilitzin, 2016). For datasets for which these quantities are believed to be important, applying the lead-lag transformation may be appropriate.

2.3.2. Augmentations

The signature by default does not define the path uniquely: it does so up to a certain equivalence class (Hambly and Lyons, 2010), due to the translation invariance property, in which

$$\text{Sig}(X + c) = \text{Sig}(X) \quad (20)$$

for constant c , and due to its invariance with respect to time reparameterisation (Lyons, 1998). That is, the signature by default is not sensitive to translations of the path nor the speed of traversal along the path. However, standard, well-explored pre-processing techniques exist that counteract these invariance properties when dealing with time series in practice. These are:

Time augmentation This pre-processing technique removes the signature’s invariance with respect to time reparameterisation, making the signature sensitive to the speed of traversal along a path in addition to its shape. It involves simply adding another dimension to the time series $\mathbf{x} \in \mathcal{S}_n(\mathbb{R}^d)$ which consists of a uniformly increasing time index $t_1 < t_2 < \dots < t_n$,

$$\mathbf{x} = (x_1, x_2, \dots, x_n) \mapsto ((t_1, x_1), (t_2, x_2), \dots, (t_n, x_n)) \in \mathcal{S}_n(\mathbb{R}^{d+1}), \quad (21)$$

denoting the times at which the points in the series occurred.

Basepoint augmentation As discussed above, the signature by default is insensitive to translations of paths. However, this invariance property can be avoided by ensuring all time series assume a common but otherwise arbitrary initial value.

2.3.3. Lifting paths with static kernels

As stated previously, the signature kernel involves *sequentialisation* of a static kernel, such that a path taking values in some set V is “lifted” into a path evolving in some feature

space \mathcal{H} . This provides the experimenter with some flexibility regarding the choice of static kernel and corresponding feature space, and allows for the use of standard and widely employed kernels, such as the linear and Gaussian RBF kernels. Throughout this paper and unless stated otherwise, we make use of the Gaussian RBF kernel as the static kernel.

3. Approximate Bayesian computation with signature transforms

Given its unique characteristics, e.g. the universal nonlinearity property, the path signature and its associated kernel are natural candidates for feature maps and discrepancy measures in ABC to handle irregularly spaced and potentially multivariate time series data. In this section we will introduce and investigate two simple, yet powerful, techniques for incorporating signatures.

3.1. Signature ABC

Though signatures are infinite-dimensional objects, we can leverage their kernel representation (see Definition 4) to compute the distance between two paths as the norm induced by the associated inner product. For two time series, \mathbf{x} and \mathbf{y} , we can treat the signature transform formally as a *summary statistic*, $\mathbf{s}(\mathbf{x}) = \text{Sig}(\mathbf{x})$, and compute

$$\rho(\mathbf{s}(\mathbf{x}), \mathbf{s}(\mathbf{y})) := \|\text{Sig}(\mathbf{x}) - \text{Sig}(\mathbf{y})\|^2 = k(\mathbf{x}, \mathbf{x}) + k(\mathbf{y}, \mathbf{y}) - 2k(\mathbf{x}, \mathbf{y}), \quad (22)$$

where, again, $k(\mathbf{x}, \mathbf{y}) = \langle \text{Sig}(\mathbf{x}), \text{Sig}(\mathbf{y}) \rangle$. The resulting distance can be computed easily using the `sigkernel`¹ package (see A.4 for an example implementation) and used either in rejection ABC, leading to the ABC posterior

$$\pi_{\text{REJ-ABC}}(\boldsymbol{\theta} \mid \mathbf{y}) \propto \pi(\boldsymbol{\theta}) \int 1 \{ \|\text{Sig}(\mathbf{x}) - \text{Sig}(\mathbf{y})\|^2 \leq \varepsilon \} p(\mathbf{x} \mid \boldsymbol{\theta}) d\mathbf{x}$$

or alternatively following the approach of Schmon et al. (2020) as a loss in the generalized approximate posterior (4), that is

$$\pi_{\text{GBI}}(\boldsymbol{\theta} \mid \mathbf{y}) \propto \pi(\boldsymbol{\theta}) \int e^{-w\|\text{Sig}(\mathbf{x}) - \text{Sig}(\mathbf{y})\|^2} p(\mathbf{x} \mid \boldsymbol{\theta}) d\mathbf{x}.$$

Monte Carlo samples in the latter can then be obtained using, for example, a pseudo-marginal approach (Beaumont, 2003; Andrieu et al., 2009). For the remainder of this paper, we will only consider standard REJ-ABC.

In both cases our method straightforwardly extends classical approaches by using the distance function (22), suggesting the term Signature ABC (S-ABC). Representing the time series with the full signature implicitly using the signature kernel trick has the additional desirable property that the signature is a sufficient statistic for the data, which we state here.

Proposition 1 (Sufficiency of Signature). *Let $\mathbf{x} = (x_{t_1}, \dots, x_{t_n}) \in \mathcal{S}_n(\mathbb{R}^d)$ be a stream of data generated by a model $p(\mathbf{x} \mid \boldsymbol{\theta})$ at fixed times $t_1 < t_2 < \dots < t_n$. Define a linear interpolation $\mathcal{I}: \mathcal{S}_n(\mathbb{R}^d) \rightarrow \mathcal{V}^1([0, T], \mathbb{R}^d)$, mapping from the space of n -streams to the space*

¹<https://github.com/crispitaagorico/sigkernel>

of paths of bounded variation, such that $X_{t_i} = x_i$ for $i = 1, \dots, n$, and X is elsewhere a linear interpolation between these points. Denote the signature of the linearly interpolated stream as $\hat{\text{Sig}}(\mathbf{x}) = \text{Sig}(\mathcal{I}(\mathbf{x}))$.

Then, the signature is a sufficient statistic for the parameter $\boldsymbol{\theta}$. That is,

$$p(\boldsymbol{\theta} \mid \hat{\text{Sig}}(\mathbf{x})) = p(\boldsymbol{\theta} \mid \mathbf{x}).$$

We defer the proof to the appendix.

3.2. Signature Regression ABC

In some circumstances, it is desirable to find low-dimensional summary statistics for use in ABC. For example, [Fearnhead and Prangle \(2012\)](#) propose the use of the posterior mean $\mathbb{E}[\boldsymbol{\theta} \mid \mathbf{y}]$ as a summary statistic for \mathbf{y} , since it is an optimal choice in that it minimises the quadratic loss between point estimates from the posterior and the true parameter. As discussed in [Section 1.1](#), this involves fitting a vector-valued regression model from a large candidate set of summary statistics to parameters $\boldsymbol{\theta}$, since this generates an estimate of the (unknown) posterior mean. The approach of [Fearnhead and Prangle \(2012\)](#) belongs to a larger class of methods for generating low-dimensional summary statistics from a large initial candidate set, sometimes termed “projection methods” ([Beaumont, 2019](#)), which also includes the partial least regression method proposed by [Wegmann et al. \(2009\)](#).

However, a significant problem with projection methods is that it is often unclear which summary statistics should be included in the initial candidate set, yet efficacy of the approach requires this initial candidate set to contain informative summaries in the first place. Contriving informative statistics thus represents a major obstacle in many inference tasks, and involves significant domain expertise, experimentation, and computational expense. Consequently, when low-dimensional summary statistics are desired, it would be preferable to bypass the manual construction of an initial candidate set of statistics in order to use projection methods.

For the case of time series models, the path signature is a natural set of summary statistics for the regression task in SA-ABC, providing a basis for learning functions on streams due to its unique universal nonlinearity property. Naive regression on the full path signature is of course impossible, since the signature is an infinite-dimensional object. However, this may once again be circumvented using the signature kernel and corresponding kernel trick (see [Definition 4](#) and [Salvi et al. \(2020\)](#)), in the following way: use the signature kernel and kernel ridge regression ([Hastie et al., 2001](#)) to implicitly regress parameters onto the *full* signature, which is in a sense equivalent to using the infinitely long path signature as the candidate set of summary statistics in semi-automatic ABC. That is, using training examples $\{\mathbf{x}_i, \boldsymbol{\theta}_i\}_{i=1}^R \sim p(\mathbf{x} \mid \boldsymbol{\theta}) \pi(\boldsymbol{\theta})$, we find a function $\hat{\boldsymbol{\theta}}^{(j)}$ in the RKHS associated with the signature kernel k , which has the following form for each component $\theta_i^{(j)}, j = 1, \dots, p$ of the p -dimensional parameters $\{\boldsymbol{\theta}_i\}_{i=1}^R$:

$$\hat{\boldsymbol{\theta}}^{(j)}(\mathbf{x}) = \sum_{i=1}^R \omega_i^{(j)} k(\mathbf{x}, \mathbf{x}_i) \quad (23)$$

with

$$\boldsymbol{\omega}^{(j)} = (\mathbf{G} + \alpha \mathbf{I})^{-1} \boldsymbol{\psi}^{(j)}, \quad \mathbf{G}_{mn} = k(\mathbf{x}_m, \mathbf{x}_n), \quad \boldsymbol{\psi}^{(j)} = \left[\theta_1^{(j)} \quad \theta_2^{(j)} \quad \dots \quad \theta_R^{(j)} \right]', \quad (24)$$

and where \mathbf{I} is a $R \times R$ identity matrix, and $\alpha \geq 0$ is a regularisation parameter to be tuned. In this sense, signatures not only provide a natural notion of distance between time series, as described in Section 3.1, but additionally provide a suitable basis for learning functions on sequences, enabling the semi-automatic construction of summary statistics. This approach to ABC is somewhat similar to that of Nakagome et al. (2013), who employ kernel ridge regression with a Gaussian RBF kernel to perform SA-ABC. Our approach differs substantially, however, in that Nakagome et al. (2013) propose the use of hand-crafted summary statistics as input to the kernel ridge regression model, while we propose the use of the full data.

Once the data is summarised using this regression model, the discrepancy between simulation and observation is then computed as the Euclidean distance between their corresponding outputs from the kernel ridge regression model. We herein refer to this approach as signature regression ABC (SR-ABC), and provide further mathematical details on this approach in Appendix A.2.

3.3. Computational complexity

Evaluating the signature kernel for two streams $\mathbf{y} \in \mathcal{S}_n(\mathbb{R}^d)$ and $\mathbf{x} \in \mathcal{S}_m(\mathbb{R}^d)$ has complexity that is linear in d and linear in the product nm (Salvi et al., 2020). However, Salvi et al. (2020) note that by parallelising the numerical computation of the signature kernel trick, which is possible on GPUs provided certain conditions are met, it is possible to reduce the computational complexity to linear in the length of the time series. In either case, this compares favourably with MMD, which has complexity $\mathcal{O}(n^2)$ (Park et al., 2016), and Wasserstein distance (WASS), which in multivariate settings is known to scale poorly with the number of data. Bernton et al. (2019), for example, note costs of order n^3 when the Hungarian algorithm is used to solve the assignment problem. Alternative algorithms with favourable performance (compared to the Hungarian algorithm) are an active area of research, however scalability with data remains a problem for the application of Wasserstein ABC in large data settings.

4. Experiments

In this section, we present experiments comparing the performance of our signature-based methods against alternative notions of distance between simulation and observation. In particular, we compare our methods, signature ABC (S-ABC) and signature regression ABC (SR-ABC), against the use of WASS (Bernton et al., 2019) and MMD (Park et al., 2016) as measures of discrepancy, along with SA-ABC (Fearnhead and Prangle, 2012).

4.1. Implementation details

For all signature kernel computations, we use the `sigkernel` package (Salvi et al., 2020). To avoid numerical instability issues in computing the signature kernel trick, we normalise the time series by dividing by the range of the simulation output when this is known or, when this is unknown, with the range of a training set or pilot runs for SR-ABC and S-ABC, respectively.

Algorithm 1: Rejection sampling scheme

Input: prior π , observation \mathbf{y} , loss function $\rho(\cdot, \cdot)$, number of particles N , final sample size $M < N$;

Result: Empirical posterior $\sum_{i=1}^M \delta_{\boldsymbol{\theta}_i}$

for $i = 1, \dots, N$ **do**

 Sample $\boldsymbol{\theta}_i \sim \pi(\boldsymbol{\theta})$;

 Simulate $\mathbf{x}_i \sim p(\mathbf{x} \mid \boldsymbol{\theta}_i)$;

 Evaluate loss $\rho(\mathbf{x}_i, \mathbf{y})$;

end

Retain the M particles $\{\boldsymbol{\theta}_i\}_{i=1}^M$ with the lowest losses

In order to remove the translation invariance and time-invariance properties of the signature, discussed in Section 2.3, we apply basepoint and time-augmentations to all time series in every experiment.

To tune the signature kernel hyperparameter and regularisation hyperparameter for SR-ABC, we perform a grid search with 5-fold cross-validation on the training set. To tune the signature kernel hyperparameter in the case of S-ABC, we use the median of all pairwise Euclidean distances between points in the observation \mathbf{y} , although we note that other approaches could be taken, such as using the same method as for SR-ABC.

Both SA-ABC and SR-ABC require training data; for both we use $R = 300$ training examples $\{\mathbf{x}_j, \boldsymbol{\theta}_j\}_{j=1}^R \sim p(\mathbf{x} \mid \boldsymbol{\theta})\pi(\boldsymbol{\theta})$. When $\pi(\cdot)$ has bounded support, we normalise the parameters $\{\boldsymbol{\theta}_i\}_{i=1}^R$ in the training set with the range of the prior in each dimension. We also tune the bandwidth parameter for the Gaussian RBF kernel employed in the MMD loss for κ 2-ABC using the median of the pairwise absolute differences between observations in \mathbf{y} , as originally recommended by Park et al. (2016).

In all experiments, WASS indicates the 1-Wasserstein distance with curve matching, which as described in Section 2 is a method for using the Wasserstein distance for time series recommended in Bernton et al. (2019). To determine the λ coefficient, we follow the guidance of Thorpe et al. (2017) and choose

$$\lambda \simeq \frac{V}{T}, \quad (25)$$

where V is the expected vertical range and T is the length of the time interval over which observations are made, in order to balance the effects of vertical and horizontal transport. Where the value of V is not apparent *a priori*, we estimate it using 2000 samples from the prior predictive distribution. Distances were computed using the Python Optimal Transport package (Flamary et al., 2021).

For all losses, we sample from the ABC posterior using the simple rejection scheme outlined in Algorithm 1 and, unless stated otherwise, use $N = 10^5$ and $M = 10^3$. While other, more sophisticated schemes exist, we choose this to facilitate a simple and transparent comparison of the different loss functions. To assess the quality of the recovered posteriors, we compute an unbiased estimate of the maximum mean discrepancy (MMD) between the approximate ground truth posteriors and empirical posteriors. A smaller MMD indicates a closer match to the approximate ground truth. To estimate the MMD between posteriors, we use a Gaussian RBF kernel with scale parameter chosen according to the median heuristic (Briol et al., 2019).

4.2. Moving average model

We consider a moving average model of order 2 (MA(2)), for which the data $\mathbf{x} = (x_t)_{t=0}^T$ are generated as

$$x_0 = 0, \tag{26}$$

$$x_1 = \epsilon_1 + \theta_1 \epsilon_0, \tag{27}$$

$$x_t = \epsilon_t + \theta_1 \epsilon_{t-1} + \theta_2 \epsilon_{t-2}, \quad t = 2, \dots, T, \tag{28}$$

with $\epsilon_t \sim \mathcal{N}(0, 1)$ and unknown parameters $\boldsymbol{\theta} = (\theta_1, \theta_2)$. We generate an observation $\mathbf{y} \sim p(\mathbf{x}|\boldsymbol{\theta}^*)$, with $\boldsymbol{\theta}^* = (0.6, 0.2)$, and assume the task of estimating $\pi(\boldsymbol{\theta}|\mathbf{y})$, using as the prior distribution a uniform distribution on the triangle defined as $\theta_1 \in [-2, 2]$, $\theta_1 + \theta_2 > -1$, $\theta_1 - \theta_2 < 1$ and $\theta_2 < 1$. Constraining the parameters to lie in this triangle guarantees identifiability of the model (Marin et al., 2012).

The likelihood for this model is available in closed-form as

$$p(\mathbf{x} | \boldsymbol{\theta}) = \mathcal{N}(\mathbf{0}, \mathbf{M}_{\boldsymbol{\theta}}), \tag{29}$$

where

$$\boldsymbol{\Sigma}_{\boldsymbol{\theta}} = \mathbf{C}\mathbf{C}^T, \quad \mathbf{C} = \begin{bmatrix} 1 & \theta_1 & \theta_2 & 0 & \dots & 0 \\ 0 & 1 & \theta_1 & \theta_2 & \ddots & 0 \\ 0 & \ddots & \ddots & \ddots & \ddots & \vdots \\ 0 & \ddots & \ddots & 1 & \theta_1 & \theta_2 \\ \vdots & \ddots & \ddots & \ddots & 1 & \theta_1 \\ 0 & 0 & 0 & \dots & 0 & 1 \end{bmatrix}, \tag{30}$$

and $\mathbf{M}_{\boldsymbol{\theta}}$ is $\boldsymbol{\Sigma}_{\boldsymbol{\theta}}$ with the last column and row removed. Consequently, an approximate ground truth posterior can be recovered in a straightforward manner with MCMC (see Appendix A.3).

In Figure 3, we show boxplots for the distribution of MMDs obtained using each loss function by running Algorithm 1 using 30 different random number generator seeds. For SA-ABC, we use the first, second, third, and fourth powers of the time series as the regressors. We see here that the signature methods that we have introduced tend to produce more accurate posterior densities than each of MMD, SA-ABC, and WASS. In particular, S-ABC with the lead-lag transformation—a common path augmentation when using path signatures (see Section 2.3)—significantly outperforms all methods considered.

We also show in Figure 4 boxplots for the distribution of squared distances between the posterior means obtained from each ABC posterior and the posterior mean recovered using Metropolis-Hastings (MH). Here we see that, in addition to increased accuracy over the entire posterior, our methods are better able to recover a more accurate point estimate in this setting than competing methods.

4.3. Geometric Brownian motion

Geometric Brownian motion (GBM) is a stochastic differential equation widely used in mathematical finance to model the dynamics of a stock price x_t evolving with time t according to

$$dx_t = \mu x_t dt + \sigma x_t dW_t, \tag{31}$$

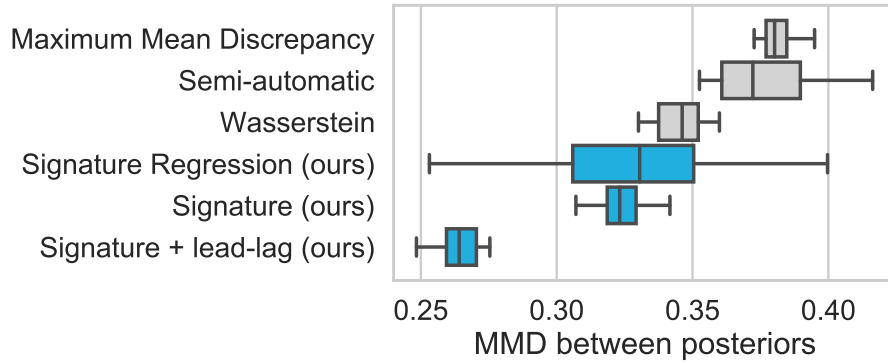


Figure 3.: (Moving average model of order 2) Maximum mean discrepancies between the ABC posteriors recovered with each choice of loss function and approximate ‘ground truth’ samples obtained using a Metropolis-Hastings random walk. Our methods are shown in blue.

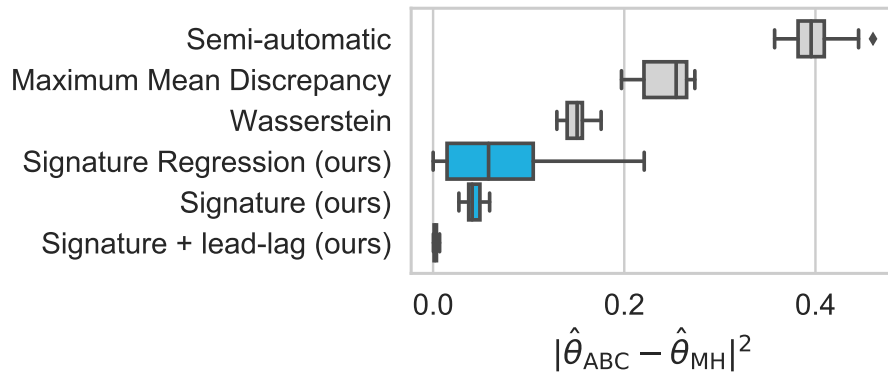


Figure 4.: (Moving average model of order 2) Squared distances between the means of the ABC posteriors and the posterior mean obtained using a Metropolis-Hastings random walk, for each loss function. Our methods are shown in blue.

where μ is the percentage drift, σ is the volatility, and W_t is a Brownian motion. This model permits an exact discretisation with $i = 1, 2, \dots, T - 1$ as

$$\log x_{i\Delta t} = \log x_{(i-1)\Delta t} + \left(\mu - \frac{1}{2}\sigma^2 \right) \Delta t + \sigma\sqrt{\Delta t} \epsilon_i, \quad (32)$$

which implicitly defines the model $p(\mathbf{x} | \boldsymbol{\theta})$ from which we simulate. For all simulations, we fix $x_0 = 10$, $T = 100$, and $\Delta t = 1/(T - 1)$.

We consider the task of recovering the posterior for parameters $\boldsymbol{\theta} = (\mu, \sigma)$ given an observation $\mathbf{y} = (y_0, y_{\Delta t}, y_{2\Delta t}, \dots, y_{(T-1)\Delta t}) \sim p(\mathbf{x} | \boldsymbol{\theta}^*)$ with $\boldsymbol{\theta}^* = (0.2, 0.5)$. We assume independent, uniform priors on the parameters as follows:

$$\mu \sim \mathcal{U}(-1, 1), \quad \sigma \sim \mathcal{U}(0.2, 2). \quad (33)$$

Inference is amenable to standard, exact likelihood-based Bayesian techniques such as MH sampling using the transition density implied by (32), enabling a comparison against an approximate ground truth posterior. For SA-ABC, we once again regress the parameters $\boldsymbol{\theta}$ onto the first, second, third, and fourth powers of the time series.

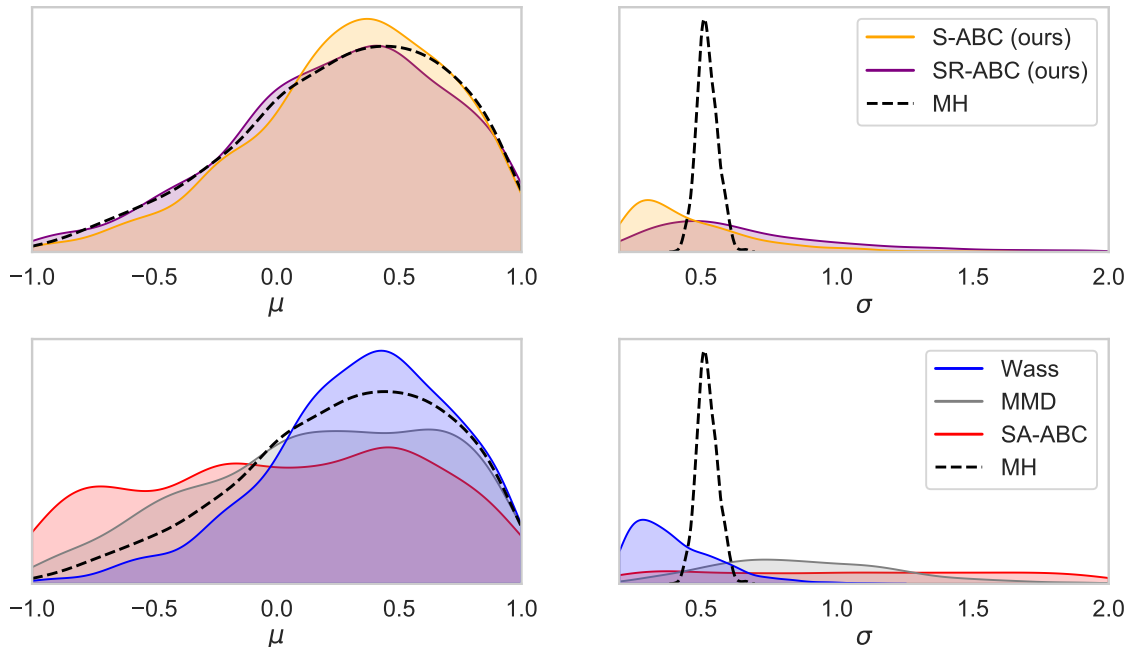


Figure 5.: (Geometric Brownian motion) Examples of the marginal posterior distributions recovered using each loss function and the approximate ground-truth posterior recovered with a Metropolis-Hastings (MH) random walk. Top: The marginal posteriors recovered using our signature methods (S-ABC and SR-ABC) and the approximate ground-truth posterior (MH). Bottom: The marginal posteriors recovered using the Wasserstein distance with curve matching (WASS), K2-ABC (MMD), and semi-automatic ABC with powers of the observations as regressors (SA-ABC).

We show in Figure 5 the marginal posteriors recovered using the Metropolis-Hastings (MH) approximation (see Appendix A.3 for details) using the true likelihood function, along with the approximate posteriors obtained using the rejection sampling scheme in Algorithm 1 and each of the four loss functions considered. Of all methods, we see that S-ABC and SR-ABC track the approximate ground truth marginal posterior generated by MH for μ most

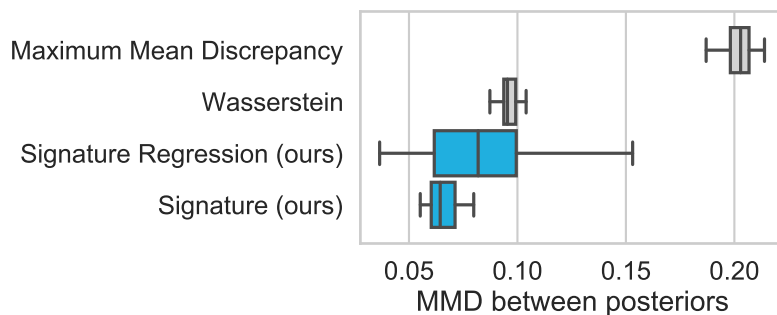


Figure 6.: (Geometric Brownian motion) Maximum mean discrepancies between the ABC posteriors recovered from each loss function and approximate ground truth samples obtained using a Metropolis-Hastings random walk. Our methods are shown in blue. Semi-automatic ABC is uniformly worse and is omitted for clarity.

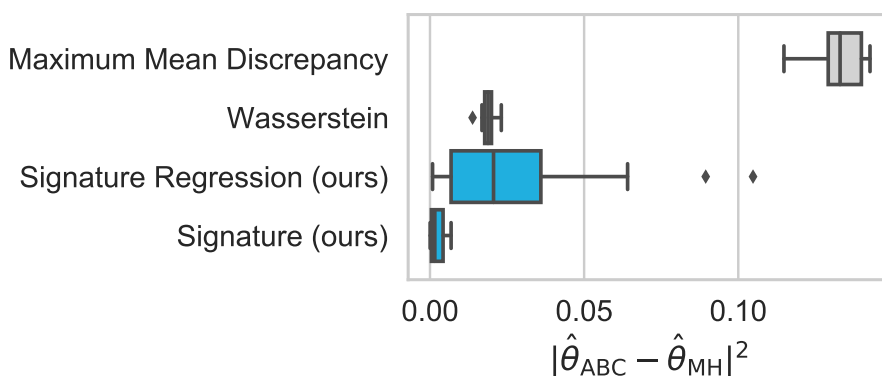


Figure 7.: (Geometric Brownian motion) Squared distances between the means of the ABC posteriors and the posterior mean obtained using a Metropolis-Hastings random walk, for each loss function. Our methods are shown in blue.

closely, and are the most concentrated around the neighbourhood of the true marginal posterior for σ .

We further show in Figure 6 boxplots of the MMDs between the posteriors recovered using each loss function and the approximate ground truth over 20 seeds. (We omit SA-ABC for clarity, since the MMDs of the posteriors recovered with this method are significantly larger than those of the other methods shown.) We see here that the closer match to the approximate ground truth posterior is also manifested as lower values of MMDs between posteriors, indicating that the shape of the joint distribution over (μ, σ) is also more accurately recovered using the signature methods.

Additionally, in Figure 7, we show boxplots for the distribution of squared distances between the posterior means obtained from each ABC posterior and the posterior mean recovered using MH. We once again omit SA-ABC for clarity, since the squared distances were significantly larger for this method. We see here that both signature methods produce estimates of the posterior mean that are significantly more accurate those obtained with MMD. Furthermore, we see that SR-ABC frequently produces estimates that are more accurate than WASS, while S-ABC does so consistently and by a significant margin.

4.4. Ricker model

The Ricker model is a simple model of ecological dynamics that exhibits chaotic behaviour and has an intractable likelihood function. The state of the model, which tracks the size N_t of a population over discrete time steps t , evolves as

$$\log N_{t+1} = \log r + \log N_t - N_t + \sigma \epsilon_t, \quad (34)$$

where $r > 0$ is a growth parameter and $\epsilon_t \sim \mathcal{N}(0, 1)$. Following Wood (2010), we assume Poissonian observations

$$y_t \sim \text{Po}(\phi N_t), \quad (35)$$

where $\phi > 0$ is a scale parameter. We assume the task of recovering the posterior distribution for $\boldsymbol{\theta} = (\log r, \phi, \sigma)$ given a time series of length $T = 50$, $\mathbf{y} = (y_1, y_2, \dots, y_T) \sim p(\mathbf{x}|\boldsymbol{\theta}^*)$ with $\boldsymbol{\theta}^* = (4, 10, 0.3)$. We take $N_0 = 1$. We further assume the following independent, uniform priors for each parameter:

$$\log r \sim \mathcal{U}(3, 8), \quad (36)$$

$$\phi \sim \mathcal{U}(0, 20), \quad (37)$$

$$\sigma \sim \mathcal{U}(0, 0.6). \quad (38)$$

The time series generated by the Ricker model tend to consist of many zero terms, with occasional spikes. For this reason, we use the cumulative sum pre-signature transformation (see Section 2.3) for s-ABC, which is a common transformation for spiking data such as medical data (Morrill et al., 2019). For SA-ABC, the hand-crafted summary statistics we use are those proposed in Wood (2010), and consist of: the autocovariances to lag 5; the mean; the number of zeros in the sequence; the coefficients of the regression $x_{t+1}^{0.3} = \beta_1 x_t^{0.3} + \beta_2 x_t^{0.6} + \epsilon_t$ for error term ϵ_t ; and the coefficients of the cubic regression of the ordered differences $x_t - x_{t-1}$ on their observed values.

In Figure 8, we show boxplots for the MMDs between the recovered posteriors and an approximation of the true posterior obtained using particle Markov chain Monte Carlo (PMCMC) (Andrieu et al., 2010, see Appendix A.3 for details). For this experiment, we run each inference procedure 30 times with different seeds. We see that the two signature-based methods once again tend to produce better estimates of the approximate ground truth posterior than MMD and WASS. SA-ABC performs particularly well in this example as it uses hand-crafted summary statistics. However, the potential power of signature-based methods is demonstrated by SR-ABC outperforming SA-ABC, despite the latter using summary statistics carefully engineered by experts.

In Figure 9, we show boxplots for the squared distances between the posterior means obtained from each ABC posterior and the posterior mean recovered using PMCMC. In this example, while MMD performed comparatively poorly in terms of its ability to recover the shape of the posterior density, it is able to recover the true posterior mean more accurately than all other methods. However, of the remaining methods considered, we once again observe more accurate estimates of the true posterior mean using our signature-based methods than using WASS and SA-ABC, despite the use of summary statistics hand-crafted by experts in the latter case.

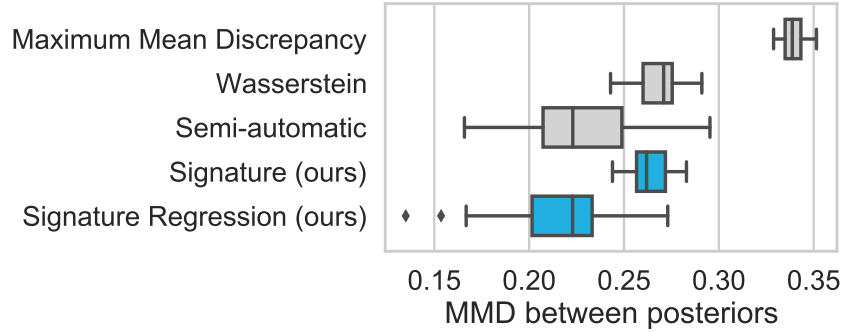


Figure 8.: (Ricker model) Maximum mean discrepancies between the posteriors recovered from the different loss functions and an approximate ground truth obtained using PMCMC. Our methods are shown in blue.

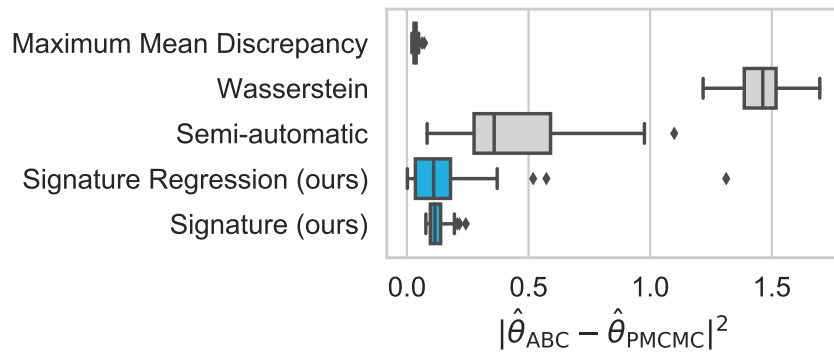


Figure 9.: (Ricker model) Squared distances between the means of the ABC posteriors and the posterior mean obtained using a PMCMC, for each loss function. Our methods are shown in blue.

4.5. An example of irregular, multivariate data: generalised stochastic epidemics

As previously discussed, the signature method naturally allows for inference with multivariate time series. To demonstrate this, we consider a generalised stochastic epidemic model (Kypraios, 2007), which simulates the spread of an infection through a fixed population of N individuals. Individuals are initially susceptible, may become infected, and subsequently recover without the possibility of reinfection. Dynamics of the model are determined by parameters β and γ , which control the rate of infection and recovery according to the following transition probabilities:

$$P[X_{t+\delta t} - X_t = -1, Y_{t+\delta t} - Y_t = 1 \mid \mathcal{H}_t] = \beta X_t Y_t \delta t + o(\delta t), \quad (39)$$

$$P[X_{t+\delta t} - X_t = 0, Y_{t+\delta t} - Y_t = -1 \mid \mathcal{H}_t] = \gamma Y_t \delta t + o(\delta t), \quad (40)$$

$$P[X_{t+\delta t} - X_t = 0, Y_{t+\delta t} - Y_t = 0 \mid \mathcal{H}_t] = 1 - \beta X_t Y_t \delta t + \gamma Y_t \delta t + o(\delta t), \quad (41)$$

where X_t and Y_t are the number of susceptible and infected individuals at time $t \in [0, T]$, respectively, and \mathcal{H}_t is a sigma-algebra generated by the process up until time t . These three transition probabilities thus capture infection, recovery, and an absence of activity, respectively.

We consider the problem of recovering the posterior density for $\boldsymbol{\theta} = (\beta, \gamma)$ given observations of the infections and recoveries occurring in the observation period $[0, T]$ with $T = 50$ in a system of $Z = 100$ individuals. For every simulation, the epidemic begins with one infected individual at time $t = 0$. We generate “empirical” data at parameters $\boldsymbol{\theta}^* = (10^{-2}, 10^{-1})$, and assume Gamma priors for both β and γ ,

$$\beta \sim \Gamma(\lambda_\beta, \nu_\beta), \quad (42)$$

$$\gamma \sim \Gamma(\lambda_\gamma, \nu_\gamma), \quad (43)$$

with $\lambda_\beta = 0.1$, $\nu_\beta = 2$, $\lambda_\gamma = 0.2$, and $\nu_\gamma = 0.5$. It can be shown (Kypraios, 2007) that this prior is conjugate for the model, leading to the posterior density

$$\pi(\beta, \gamma \mid \mathbf{I}, \mathbf{R}) \propto \beta^{\lambda_\beta + n_I - 2} \exp \left\{ -\beta \left(\int_{\phi_1}^T X_t Y_t dt + \nu_\beta \right) \right\} \gamma^{\lambda_\gamma + n_R - 1} \exp \left\{ -\gamma \left(\int_{\phi_1}^T Y_t dt + \nu_\gamma \right) \right\}, \quad (44)$$

where \mathbf{I} and \mathbf{R} are the infection and recovery times, respectively, n_I and n_R are the total number of individuals in the model that are infected and that recover over the course of the simulation, respectively, and ϕ_1 is the time of the first infection. Thus, samples can be drawn from the exact posterior for a given dataset simulated by this model. We simulate the model using the Gillespie algorithm (Gillespie, 1977), such that the number of increments in the simulated sequences is also random.

To perform s-ABC, we bring all three channels of the multivariate stream—number of infected individuals, number of recovered individuals, and time—into the range $[0, 1]$ by dividing by Z , Z , and T , respectively.

We show in Figure 10 plots for the distribution of MMDs between samples from the approximate posteriors generated with WASS and s-ABC and samples from the ground truth exact posterior. To obtain these approximate posteriors, we use Algorithm 1 with $N = 5 \times 10^5$ and $M = 100$. We also show boxplots for the distribution of squared

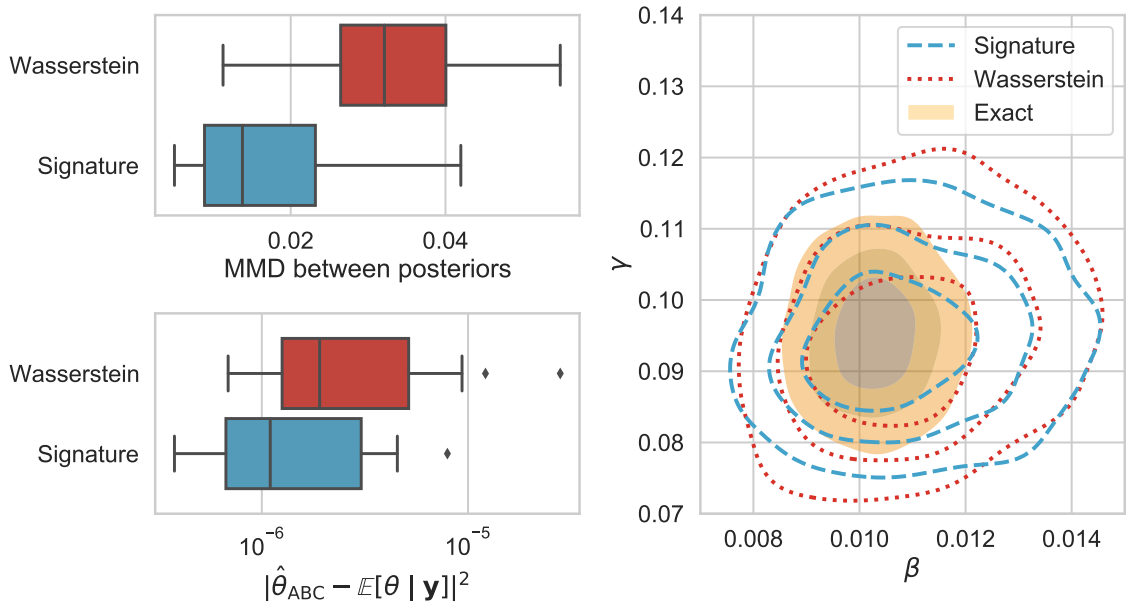


Figure 10.: (Generalised stochastic epidemic model) Top left: Maximum mean discrepancies between the posteriors recovered from Wasserstein + curve matching (red) and Signature (blue) loss functions over 25 seeds and samples from the exact posterior. Bottom left: Squared distances between the means of the ABC posteriors and the true posterior mean. Our method is in blue. Right: An example of the joint posterior densities recovered with Wasserstein + curve matching (red) and the Signature ABC (blue), and samples from the exact posterior (orange).

distances between the posterior means obtained with WASS and S-ABC and the exact posterior mean. On the right hand side of the figure, we show contour plots obtained by running the inference procedure with 25 different seeds and pooling the best M losses, and compare these against samples from the ground truth posterior, (44). From all of this, we see that the natural notion of distance between multivariate and irregularly sampled time series data of different lengths, enabled by the use of path signatures, manifests as better recovery of both the true posterior distribution and the true posterior mean in this example, in which the MMDs between posteriors and squared distances between posterior means for S-ABC are generally lower than those obtained using WASS. This is apparent in the posterior density plot also, in which we see greater concentration around the true posterior density using S-ABC than WASS.

5. Conclusion

In this paper, we introduced two novel approaches—Signature ABC and Signature Regression ABC—to performing approximate Bayesian computation with time series simulation models. Each method relies on the recently developed signature kernel trick to compute discrepancies between time series data. As an illustration of our proposed methods, we presented four examples of Bayesian inference tasks in which our approaches outperform existing techniques that are common in the approximate Bayesian inference literature. We demonstrate that our methods flexibly accommodate a number of potentially helpful transformations of the data, for example the lead-lag transformation (Flint et al., 2016),

and in our final example that our methods are immediately applicable to multivariate and irregularly sampled time series data.

While we have compared the different loss functions using a basic rejection algorithm in this paper in order to allow for a simple and transparent comparison, we note that our proposed methods can be embedded within other more sophisticated sampling algorithms, for example MCMC or sequential Monte Carlo methods. Additionally for the Signature Regression ABC method, there is the possibility of incorporating mechanisms for generating more accurate regression results, for example using a pilot run to determine regions of non-negligible posterior mass as described in [Fearnhead and Prangle \(2012\)](#). This may allow for improved approximations to the true posterior density.

6. Acknowledgements

The authors thank James Morrill, Cristopher Salvi, Zacharia Issa, Horatio Boedihardjo and Lajos Gergely Gyurko for helpful discussions. JD is supported by the EPSRC Centre For Doctoral Training in Industrially Focused Mathematical Modelling (EP/L015803/1) in collaboration with Improbable.

References

- Justin Alsing, Benjamin Wandelt, and Stephen Feeney. Massive optimal data compression and density estimation for scalable, likelihood-free inference in cosmology. *Monthly Notices of the Royal Astronomical Society*, 477(3):2874–2885, Mar 2018. ISSN 1365-2966. doi: 10.1093/mnras/sty819. URL <http://dx.doi.org/10.1093/mnras/sty819>.
- Christophe Andrieu, Gareth O Roberts, et al. The pseudo-marginal approach for efficient monte carlo computations. *The Annals of Statistics*, 37(2):697–725, 2009.
- Christophe Andrieu, Arnaud Doucet, and Roman Holenstein. Particle markov chain monte carlo methods. *Journal of the Royal Statistical Society: Series B (Statistical Methodology)*, 72(3):269–342, 2010.
- Mark A Beaumont. Estimation of population growth or decline in genetically monitored populations. *Genetics*, 164(3):1139–1160, 2003.
- Mark A Beaumont. Approximate bayesian computation. *Annual review of statistics and its application*, 6:379–403, 2019.
- Mark A Beaumont, Wenyang Zhang, and David J Balding. Approximate bayesian computation in population genetics. *Genetics*, 162(4):2025–2035, 2002.
- Espen Bernton, Pierre E. Jacob, Mathieu Gerber, and Christian P. Robert. Approximate Bayesian computation with the Wasserstein distance. *Journal of the Royal Statistical Society. Series B: Statistical Methodology*, 81(2):235–269, 2019. ISSN 14679868. doi: 10.1111/rssb.12312.
- Pier Giovanni Bissiri, Chris C Holmes, and Stephen G Walker. A general framework for updating belief distributions. *Journal of the Royal Statistical Society. Series B, Statistical methodology*, 78(5):1103, 2016.

- Patric Bonnier *et al.* Deep signature transforms. *Neural Information Processing Systems*, 2019.
- Elizabeth Bradley and Holger Kantz. Nonlinear time-series analysis revisited. *Chaos: An Interdisciplinary Journal of Nonlinear Science*, 25(9):097610, Sep 2015. ISSN 1089-7682. doi: 10.1063/1.4917289. URL <http://dx.doi.org/10.1063/1.4917289>.
- François Xavier Briol, Alessandro Barp, Andrew B. Duncan, and Mark Girolami. Statistical inference for generative models with maximum mean discrepancy. *arXiv*, pages 1–57, 2019.
- Ilya Chevyrev and Andrey Kormilitzin. A Primer on the Signature Method in Machine Learning. 2016. URL <http://arxiv.org/abs/1603.03788>.
- Ilya Chevyrev and Harald Oberhauser. Signature moments to characterize laws of stochastic processes, 2018.
- Kim Christensen, Kishan A. Manani, and Nicholas S. Peters. Simple model for identifying critical regions in atrial fibrillation. *Physical Review Letters*, 114(2):1–6, 2015. ISSN 10797114. doi: 10.1103/PhysRevLett.114.028104.
- Christopher Drovandi and David T Frazier. A comparison of likelihood-free methods with and without summary statistics. *arXiv preprint arXiv:2103.02407*, 2021.
- Paul Fearnhead and Dennis Prangle. Constructing summary statistics for approximate Bayesian computation: Semi-automatic approximate Bayesian computation. *Journal of the Royal Statistical Society. Series B: Statistical Methodology*, 74(3):419–474, 2012. ISSN 13697412. doi: 10.1111/j.1467-9868.2011.01010.x.
- Rémi Flamary, Nicolas Courty, Alexandre Gramfort, Mokhtar Z. Alaya, Aurélie Boisbunon, Stanislas Chambon, Laetitia Chapel, Adrien Corenflos, Kilian Fatras, Nemo Fournier, Léo Gautheron, Nathalie T.H. Gayraud, Hicham Janati, Alain Rakotomamonjy, Ievgen Redko, Antoine Rolet, Antony Schutz, Vivien Seguy, Danica J. Sutherland, Romain Tavenard, Alexander Tong, and Titouan Vayer. Pot: Python optimal transport. *Journal of Machine Learning Research*, 22(78):1–8, 2021. URL <http://jmlr.org/papers/v22/20-451.html>.
- Guy Flint, Ben Hambly, and Terry Lyons. Discretely sampled signals and the rough hof process. *Stochastic Processes and their Applications*, 126(9):2593–2614, 2016. ISSN 0304-4149. doi: <https://doi.org/10.1016/j.spa.2016.02.011>. URL <https://www.sciencedirect.com/science/article/pii/S0304414916000429>.
- Andrew M. Fraser and Harry L. Swinney. Independent coordinates for strange attractors from mutual information. *Phys. Rev. A*, 33:1134–1140, Feb 1986. doi: 10.1103/PhysRevA.33.1134. URL <https://link.aps.org/doi/10.1103/PhysRevA.33.1134>.
- John Geanakoplos, Robert Axtell, J. Doyne Farmer, Peter Howitt, Benjamin Conlee, Jonathan Goldstein, Matthew Hendrey, Nathan M. Palmer, and Chun-Yi Yang. Getting at systemic risk via an agent-based model of the housing market. *American Economic Review*, 102(3):53–58, May 2012. doi: 10.1257/aer.102.3.53. URL <https://www.aeaweb.org/articles?id=10.1257/aer.102.3.53>.
- Daniel T. Gillespie. Exact stochastic simulation of coupled chemical reactions. *The Journal of Physical Chemistry*, 81(25):2340–2361, 1977. doi: 10.1021/j100540a008. URL <https://doi.org/10.1021/j100540a008>.

- Lajos Gergely Gyurk. Extracting information from the signature of a financial data stream. pages 1–22, 2014.
- Ben Hambly and Terry Lyons. Uniqueness for the signature of a path of bounded variation and the reduced path group. *Annals of Mathematics*, 171(1):109–167, Mar 2010. ISSN 0003-486X. doi: 10.4007/annals.2010.171.109. URL <http://dx.doi.org/10.4007/annals.2010.171.109>.
- Trevor Hastie, Robert Tibshirani, and J. H Friedman. *The elements of statistical learning : data mining, inference, and prediction*. Springer series in statistics. Springer, New York, 2001. ISBN 9780387952840.
- Franz J. Király and Harald Oberhauser. Kernels for sequentially ordered data. *Journal of Machine Learning Research*, 20:1–45, 2019. ISSN 15337928.
- Jeremias Knoblauch, Jack Jewson, and Theodoros Damoulas. Generalized variational inference: Three arguments for deriving new posteriors. *arXiv preprint arXiv:1904.02063*, 2019.
- Theo Kypraios. Efficient bayesian inference for partially observed stochastic epidemics and a new class of semi-parametric time series models. 2007.
- Daniel Levin, Terry Lyons, and Hao Ni. Learning from the past, predicting the statistics for the future, learning an evolving system, 2016.
- Chenyang Li, Xin Zhang, and Lianwen Jin. LPSNet: A Novel Log Path Signature Feature Based Hand Gesture Recognition Framework. *Proceedings - 2017 IEEE International Conference on Computer Vision Workshops, ICCVW 2017*, 2018-January:631–639, 2017. doi: 10.1109/ICCVW.2017.80.
- Terry Lyons. Differential equations driven by rough signals. 1998.
- Terry Lyons. Rough paths, Signatures and the modelling of functions on streams. (291244), 2014a. URL <http://arxiv.org/abs/1405.4537>.
- Terry Lyons. Rough paths, signatures and the modelling of functions on streams. *arXiv preprint arXiv:1405.4537*, 2014b.
- Jean Michel Marin, Pierre Pudlo, Christian P. Robert, and Robin J. Ryder. Approximate Bayesian computational methods. *Statistics and Computing*, 22(6):1167–1180, 2012. ISSN 09603174. doi: 10.1007/s11222-011-9288-2.
- P. J. Moore, T. J. Lyons, and J. Gallacher. Using path signatures to predict a diagnosis of Alzheimer’s disease. *PLoS ONE*, 14(9):1–16, 2019. ISSN 19326203. doi: 10.1371/journal.pone.0222212. URL <http://dx.doi.org/10.1371/journal.pone.0222212>.
- James Morrill, Andrey Kormilitzin, Alejo Nevado-Holgado, Sumanth Swaminathan, Sam Howison, and Terry Lyons. The Signature-Based Model for Early Detection of Sepsis from Electronic Health Records in the Intensive Care Unit. *Computing in Cardiology*, 2019-Sept:2–5, 2019. ISSN 2325887X. doi: 10.23919/CinC49843.2019.9005805.
- James Morrill, Adeline Fermanian, Patrick Kidger, and Terry Lyons. A generalised signature method for time series. *arXiv preprint*, 2020.
- Shigeki Nakagome, Kenji Fukumizu, and Shuhei Mano. Kernel approximate bayesian computation in population genetic inferences. *Statistical Applications in Genetics and Molecular Biology*, 12(6):667–678, 2013. doi: doi:10.1515/sagmb-2012-0050. URL <https://doi.org/10.1515/sagmb-2012-0050>.

- Mijung Park, Wittawat Jitkrittum, and Dino Sejdinovic. K2-ABC: Approximate bayesian computation with kernel embeddings. *Proceedings of the 19th International Conference on Artificial Intelligence and Statistics, AISTATS 2016*, 41:398–407, 2016.
- Dennis Prangle. Summary statistics in approximate bayesian computation. In Scott A Sisson, Yanan Fan, and Mark Beaumont, editors, *Handbook of approximate Bayesian computation*, pages 125–152. FL: CRC, 2018.
- Jonathan K Pritchard, Mark T Seielstad, Anna Perez-Lezaun, and Marcus W Feldman. Population growth of human Y chromosomes: a study of Y chromosome microsatellites. *Molecular biology and evolution*, 16(12):1791–1798, 1999.
- Cristopher Salvi, Thomas Cass, James Foster, Terry Lyons, and Weixin Yang. The signature kernel is the solution of a goursat pde. *arXiv preprint arXiv:2006.14794*, 2020.
- M.J. Schervish. *Theory of Statistics*. Springer series in statistics. 3Island Press, 1995. ISBN 9781461242512. URL <https://books.google.co.uk/books?id=fv0CoAEACAAJ>.
- S M Schmon, G Deligiannidis, A Doucet, and M K Pitt. Large-sample asymptotics of the pseudo-marginal method. *Biometrika*, 108(1):37–51, 03 2021. ISSN 0006-3444. doi: 10.1093/biomet/asaa044. URL <https://doi.org/10.1093/biomet/asaa044>.
- Sebastian M Schmon and Philippe Gagnon. Optimal scaling of random walk metropolis algorithms using bayesian large-sample asymptotics. *arXiv preprint arXiv:2104.06384*, 2021.
- Sebastian M Schmon, Patrick W Cannon, and Jeremias Knoblauch. Generalized posteriors in approximate bayesian computation. *arXiv preprint arXiv:2011.08644*, 2020.
- Simon Tavaré, David J Balding, Robert C Griffiths, and Peter Donnelly. Inferring coalescence times from dna sequence data. *Genetics*, 145(2):505–518, 1997.
- Matthew Thorpe, Serim Park, Soheil Kolouri, Gustavo K Rohde, and Dejan Slepčev. A Transportation L^p Distance for Signal Analysis. *Journal of mathematical imaging and vision*, 59(2):187–210, 2017.
- Csaba Toth and Harald Oberhauser. Variational Gaussian Processes with Signature Covariances. 2019. URL <http://arxiv.org/abs/1906.08215>.
- Daniel Wegmann, Christoph Leuenberger, and Laurent Excoffier. Efficient Approximate Bayesian Computation Coupled With Markov Chain Monte Carlo Without Likelihood. *Genetics*, 182(4):1207–1218, 08 2009. ISSN 1943-2631. doi: 10.1534/genetics.109.102509. URL <https://doi.org/10.1534/genetics.109.102509>.
- Simon N. Wood. Statistical inference for noisy nonlinear ecological dynamic systems. *Nature*, 466(7310):1102–1104, 2010. ISSN 00280836. doi: 10.1038/nature09319.
- Zecheng Xie, Zenghui Sun, Lianwen Jin, Hao Ni, and Terry Lyons. Learning Spatial-Semantic Context with Fully Convolutional Recurrent Network for Online Handwritten Chinese Text Recognition. *IEEE Transactions on Pattern Analysis and Machine Intelligence*, 40(8):1903–1917, 2018. ISSN 01628828. doi: 10.1109/TPAMI.2017.2732978.

A. Appendix

A.1. Proof of Proposition 1

Proof. Trivially \mathbf{x} is its own sufficient statistic, and it follows from the Fisher-Neyman factorization theorem (see, e.g., [Schervish, 1995](#), Theorem 2.21) that an injective function of a sufficient statistic is also sufficient. Therefore, it remains to show injectivity of the map $\mathbf{x} \mapsto \hat{\text{Sig}}(\mathbf{x})$. We do this by establishing injectivity of $\mathcal{I}(\cdot)$ and $\text{Sig}(\cdot)$, since $\hat{\text{Sig}}(\mathbf{x})$ is a composition of these functions, and the composition of two injective functions is injective.

It follows immediately from the definition that $\mathbf{x} \mapsto \mathcal{I}(\mathbf{x})$ is injective for $\mathbf{x} \in \mathcal{S}_n(\mathbb{R}^d)$. Since $X = \mathcal{I}(\mathbf{x})$ is a linear interpolation of a bounded stream, it is naturally of finite 1-variation. Further, we have assumed it has a fixed starting point and at least one monotone coordinate. Therefore its signature is unique ([Levin et al., 2016](#), Lemma 2.14), and $\text{Sig} : \mathcal{V}^1([0, T], \mathbb{R}^d) \rightarrow T((\mathbb{R}^d))$ defines an injection, where $T((\mathbb{R}^d))$ is the tensor algebra space

$$T((\mathbb{R}^d)) := \left\{ (a_0, a_1, \dots, a_n, \dots) \mid \forall n \geq 0, a_n \in (\mathbb{R}^d)^{\otimes n} \right\}.$$

□

A.2. Signature Regression ABC

For SR-ABC, we proceed as follows:

1. fit a kernel ridge regression model using training data $\{\mathbf{x}_i, \boldsymbol{\theta}_i\}_{i=1}^R \sim p(\mathbf{x}, \boldsymbol{\theta})$. This amounts to solving the following optimisation problem for each of the p components $j = 1, \dots, p$ of the $\{\boldsymbol{\theta}_i\}_{i=1}^R$:

$$\min_{\hat{\boldsymbol{\theta}}^{(j)} \in \mathcal{H}_k} \sum_{i=1}^R \left(\theta_i^{(j)} - \hat{\boldsymbol{\theta}}^{(j)}(\mathbf{x}_i) \right)^2 + \alpha \|\hat{\boldsymbol{\theta}}^{(j)}\|_{\mathcal{H}_k}^2, \quad (45)$$

where k is the signature kernel, \mathcal{H}_k is the RKHS associated with k , $\hat{\boldsymbol{\theta}}^{(j)}$ is a function of the form

$$\hat{\boldsymbol{\theta}}^{(j)}(\mathbf{x}) = \sum_{i=1}^R \omega_i^j k(\mathbf{x}, \mathbf{x}_i) \quad (46)$$

with

$$\boldsymbol{\omega}^j = (\mathbf{G} + \alpha \mathbf{I})^{-1} \boldsymbol{\psi}^{(j)}, \quad \mathbf{G}_{mn} = k(\mathbf{x}_m, \mathbf{x}_n), \quad \boldsymbol{\psi}^{(j)} = \left[\theta_1^{(j)} \quad \theta_2^{(j)} \quad \dots \quad \theta_R^{(j)} \right]', \quad (47)$$

\mathbf{I} is a $R \times R$ identity matrix, and $\alpha \geq 0$ is a regularisation parameter;

2. summarise the observation \mathbf{y} and all future simulations $\mathbf{x} \sim p(\mathbf{x}|\boldsymbol{\theta})$ using this trained kernel ridge regression model, i.e. use

$$\mathbf{s}(\mathbf{x}) = \left[\hat{\boldsymbol{\theta}}^{(1)}(\mathbf{x}) \quad \hat{\boldsymbol{\theta}}^{(2)}(\mathbf{x}) \quad \dots \quad \hat{\boldsymbol{\theta}}^{(p)}(\mathbf{x}) \right]'; \quad (48)$$

3. use the squared difference between the summaries of \mathbf{y} and \mathbf{x} as the measure of discrepancy between simulation and observation,

$$\rho\{\mathbf{s}(\mathbf{y}), \mathbf{s}(\mathbf{x})\} = \|\mathbf{s}(\mathbf{y}) - \mathbf{s}(\mathbf{x})\|_2^2. \quad (49)$$

A.3. Reference Posteriors using MCMC

Metropolis-Hastings For the moving average model of order 2 (MA(2)) and the geometric Brownian motion (GBM) model we obtain samples from this ground truth posterior using Metropolis-Hastings (MH). We follow the guidelines of [Schmon and Gagnon \(2021\)](#) and use a multivariate normal proposal, for which we estimate the covariance matrix using a pilot run. We subsequently tune the MH algorithm according to [Schmon and Gagnon \(2021, Table 1\)](#) and run the MH for 10^5 steps, keeping a thinned subset of 10^3 samples as our baseline.

Particle MCMC To obtain samples from the ground truth posterior of the Ricker model we employ particle Markov chain Monte Carlo (PMCMC) using a simple bootstrap particle filter. We follow the guidelines of [Schmon et al. \(2021\)](#), first estimating the posterior covariance in a shorter prior run and then tuning the random walk proposal as well as the particle filter to follow the [Schmon et al. \(2021, Table 1\)](#). PMCMC commonly exhibits worse convergence behaviour than standard MH and hence we run the algorithm for 2×10^5 iterations eventually retaining a thinned subset of 10^3 samples as our baseline.

A.4. Example code for Signature ABC

The distance function (22) can be computed easily with the `sigkernel` package ([Salvi et al., 2020](#)). We offer the following as an example:

```
1 import model # The simulator
2 import sigkernel # For computing the signature kernel
3
4 # Generate observation
5 y = model.simulate()
6
7 # Specify static kernel, which is sequentialised in the signature kernel
8 static_kernel = sigkernel.LinearKernel()
9
10 # Choose the dyadic order for the finite element PDE solver (integer,
11 # default is 0, higher values give more accurate PDE solutions but
12 # are more expensive)
13 dyadic_order = 0
14
15 # Sequentialise the above static kernel to create a signature kernel
16 signature_kernel = sigkernel.SigKernel(static_kernel, dyadic_order)
17 k = signature_kernel.compute_kernel
18
19 # Compute distance between simulation and observation
20 x = model.simulate()
21 distance = k(x, x) + k(y, y) - 2*k(x, y)
```

Listing 1.: Example python code for computing the distance between signatures.